Volume 1 | Number 1 | Jan 2013 | Pages 1–100

Nanoscale

www.rsc.org/nanoscale

ROYAL SOCIETY OF CHEMISTRY

ROYAL SOCIETY OF CHEMISTRY

www.rsc.org/nanoscale

Journal Name

ARTICLE

Selective GaSb Radial Growth on Crystal Phase Engineered InAs Nanowires

Luna Namazi[a], Malin Nilsson[a], Sebastian Lehmann[a], Claes Thelander[a], Kimberly A. Dick[a, b],

In this work we have developed InAs nanowire templates, with designed zinc blende and wurtzite segments, for selective growth of radial GaSb heterostructures using metal organic vapor phase epitaxy. We find that the radial growth rate of GaSb is determined by the crystal phase of InAs, and that growth is suppressed on InAs segments with pure wurtzite crystal phase. The morphology and the thickness of the grown shell can be tuned with full control by growth conditions. We demonstrate that multiple distinct core-shell segments can be designed and realized with precise control over their length and axial position. Electrical measurements confirm that suppression of shell growth is possible on segments with wurtzite structures. This growth method enables new functionalities in structures formed by bottom-up techniques, which are more complex to attain by top-down techniques.

Introduction

Semiconductor nanowires are nowadays considered to be promising candidates as building blocks in future electrical and optical devices due to their tunable physical and material properties [1]–[8]. Among them, heterostructure nanowires are of considerable importance, giving the possibility to combine desired properties of two or more different materials with minimal strain compared to conventional layers of the same materials [9]. These heterostructures can be grown either axially or radially based on device requirements. Both axial [10]–[12] and radial [13]–[15] heterostructure growth have been extensively investigated with a high degree of control of interfaces and composition. It has also been demonstrated that radial growth can be tuned to be selective to certain nanowire facets [16]. However, the unique prospect of selective radial heterostructure growth on designed axial sections along the length of the nanowire is yet to be explored and employed in a device structure. In a number of studies it has been observed that the rate of radial growth strongly depends on the crystal phase of the nanowire [17], attributed to their different surface energies [18]–[20]. Controlling the crystal structure of different segments of the nanowire, and thereby, changing the surface energies of the segments formed along the axis would provide ideal templates for studying selective radial growth [17].

In this work we demonstrate highly controlled selective radial growth in the InAs-GaSb material system, on designed InAs nanowire core templates, characterized by high resolution transmission electron microscopy (TEM) and electrical measurements. The templates are based on the finding that pure zinc blende or wurtzite structures can be formed along the length of a nanowire with high precision and control by careful tuning of the growth conditions [21]–[27]. Here, the group V precursor flow has been modified to achieve the two crystal structures of the core [28].

The growth of GaSb-InAs and InAs-GaSb core-shell nanowires has been reported in [29] and [30] by means of MOVPE and MBE, respectively. These heterostructures exhibit a broken band alignment, making such junctions interesting for various device applications, such as tunnel diodes and tunnel field effect transistors (TFETs) [31][32]. Motivated by their lower-power operation and greater scalability, TFETs are believed to be one of the most promising transistor concepts for next-generation low-power integrated circuits. For radial TFET devices, the axial extent of the radial junction is directly related to the gate length. The potential for epitaxial control of such a critical device parameter, rather than having to rely on complex etch-back processes, provides an important example of the relevance of this study [2]. Furthermore, InAs-GaSb heterostructures are fundamentally interesting for quantum transport studies such as electron-hole interaction, or as candidates for topological insulators [33]–[35]. Epitaxial growth of

well-defined core-shell segments would further allow for controlled core-shell quantum dots, where the interaction of single electrons and single holes can be studied.

It is understood that zinc blende structures possess a higher surface energy compared to wurtzite structures [28][36]. Taking advantage of this knowledge, we here intentionally suppress the radial growth on the wurtzite surfaces, while enhancing it on the zinc blende structures [17]. In other words, we make use of how the low surface energies of the wurtzite side facets compared to the zinc blende side facets hinder nucleation and hence radial growth of a shell layer - GaSb in our case - at conditions where nucleation is in fact favourable on the zinc blende surfaces. The wurtzite nanowire segments have {10-10}-type side facets, predicted to have lower energy than the {110}-type facets on the corresponding zinc blende segments [37]; it should be emphasized that other side facets would have other energies and that selectivity may be different, perhaps even opposite, for certain other facet types. We demonstrate that the morphology and diameter of the grown GaSb shell on the crystal structure-designed InAs core nanowires varies, and can be tuned to preference, by changing the direct growth parameters for the GaSb (temperature, nominal V/III ratios of the precursor flows, absolute precursor molar flow, and time). Thus, based on the interesting properties and high potential of this material system, we employ it for developing the selective radial growth concept. We also show that selective growth of shell layers on specific parts of a multiple structured core nanowire is possible.

Finally, selective InAs-GaSb core-shell and reference InAs (core-only) nanowires are evaluated with electrical measurements in top-gated devices. For InAs reference nanowires it is found that both the wurtzite and zinc blende segments have unipolar, *n*-type, transport as expected, and are depleted for negative gate voltages. For the selectively overgrown core-shell nanowires, we find that zinc blende segments show ambipolar conduction in agreement with GaSb overgrowth, whereas wurtzite segments have unipolar conduction only, evidencing a suppression of the overgrowth, and the feasibility of the template method.

Methods

InAs-GaSb core-shell nanowires are grown by means of metal-organic vapour phase epitaxy (MOVPE) on Au aerosol decorated InAs (111) B substrates. The utilized Au particle diameters are 30 and 40 nm at areal densities of 1 and 2 particles per μm^{-2}. The nanowires are grown in a standard low-pressure horizontal MOVPE reactor (Aixtron 200/4). For the InAs core Trimethylindium (TMIn) and Arsine (AsH_3), and for the GaSb shell Trimethylgallium (TMGa) and Trimethylantimony (TMSb), are used as the group III and V precursors, respectively. Hydrogen is used as the carrier gas with a total flow rate of 13 l/min, at a reactor pressure of 100 mbar. After loading the InAs samples inside the reactor, the samples were annealed for 10 minutes at a temperature of 550 °C in a H_2/AsH_3 atmosphere in order to remove the native oxide from the surface of the samples. The InAs core structure was then grown at 460 °C by supplying TMIn and AsH_3. To ensure uniform nucleation, growth was initiated with a segment grown for 3 minutes with TMIn of 3.5 x 10^{-6} and AsH3 of 1.9 x 10^{-4}, before growing the wurtzite and zinc blende segments. This segment has mostly wurtzite structure with frequent stacking faults. As a general guideline, regardless of the diameter of the initial Au particle, for growing the zinc blende segments higher AsH_3 flows are used, whereas for the wurtzite segments, the group V precursor flow is reduced to a small fraction

of that of zinc blende [28]. For particles with a diameter of 40 nm the molar fractions of AsH_3 was set to 7.7 x 10^{-5} and1.5 x 10^{-2} for the wurtzite and zinc blende segments respectively, while the TMIn precursor flow was kept at 3.5 x 10^{-6} for both segments. For particles with a diameter of 30 nm the AsH_3 and TMIn molar fractions were slightly altered to 9.2 x 10^{-5} and 3.5 x 10^{-6} for wurtzite, and 1.5 x 10^{-2} and 1.9 x 10^{-5} for zinc blende, respectively. The InAs core was designed with three segments along the length, starting with a wurtzite segment, which will be referred to as WZ1 throughout this paper. A zinc blende segment was grown as the second segment (ZB), followed by a second wurtzite segment referred to as WZ2. The first segment (WZ1) is used to isolate the ZB and WZ2 segments from the substrate and stem segment; in order to understand the radial growth concept we will compare ZB and WZ2. Please take note that throughout this paper the wurtzite and zinc blende segments will be referred to in the abbreviation form on WZ and ZB, whereas whenever the discussing general topics related to these two crystal phases the full names are used. The growth times were varied based on the desired length of each segment, the initial particle diameter, and density. The effect of areal density on the length and morphology of the grown nanowires is demonstrated in S4 in the supplementary information. Typically growth times of 6 minutes for the ZB segment resulted in a length of around 500-700 nm, and 2-5 minutes for the wurtzite segments gave a length of 400-1200 nm depending on particle diameter and density. For more details of the InAs structure optimization see Supplementary Information S1.

As the next step, the GaSb shell was grown by simultaneously switching Group III and V precursors from TMIn to TMGa and AsH_3 to TMSb. The study of temperature dependence is an exception from this simultaneous switch, where the temperature was first ramped to the desired value under a constant presence of AsH_3 before switching TMGa and TMSb on. After growth all samples were cooled under a flow of H_2.

A particular set of growth conditions for the GaSb shell are defined as the initial or reference parameters, which will be referred and compared to throughout this paper. These shell-growth conditions are then mapped out, one by one, by only changing one specific parameter while keeping the others at the constant reference values. The reference molar fractions of the TMGa and TMSb precursors are 3.4 x 10^{-5} and 5.4 x 10^{-5}, respectively, resulting in a nominal V/III ratio of 1.6. The reference GaSb shell is grown at 460 °C for 20 minutes on the pre-optimized WZ1-ZB-WZ2 InAs core structure. The samples are then characterized by means of Scanning Electron Microscopy (SEM) (Zeiss LEO 1560) with typical acceleration voltages of 5-10 kV and high resolution TEM imaging (JEOL 3000F) with an acceleration voltage of 300 kV, combined with Scanning TEM X-ray energy dispersive spectroscopy (STEM-XEDS) for compositional investigations. For the TEM characterizations, the nanowires were transferred to lacey carbon-film coated copper grids by manually breaking them off from the substrate. For the TEM and XEDS analysis 4-5 nanowires were characterized with electron beam directions parallel the <110>- or <112>-type zone axes, respectively. For electrical characterization, source-, drain-, and gate contacts were processed on two sets of nanowires with axial WZ1-ZB-WZ2 segments; (i) InAs only, and (ii) with selective GaSb radial overgrowth (30 nm Au diameter, with a shell thickness of approximately 15 nm). The nanowires were mechanically transferred from the growth substrate to silicon substrates covered with a 110 nm thick SiO_2 layer and with pre-defined gold patterns to facilitate contact design. Source and drain contacts were then processed using electron beam lithography with PMMA 950 A5 as resist. After development of the resist an O_2-

plasma etch (30 s) was used to remove resist residue and directly before metal evaporation of 25/75 nm Ni/Au, an HCl:H$_2$O etch (1:20) for 10 s was performed to remove native oxide on the nanowires. After metal lift-off, remaining resist residues were removed in a second O$_2$-plasma etch step (30 s). An approximately 7 nm thick HfO$_2$ gate dielectric layer was deposited by means of atomic layer deposition at 100 °C. Windows were opened in the oxide using focused ion beam milling, to connect the top gate contacts to the pre-defined gold pads on the substrate. Finally, the top gate was processed using a similar lift-off process as for the source- and drain contacts, omitting the wet etch step prior to metallization.

Results

I.   Morphology and structure of selective InAs-GaSb core-shell nanowires

The morphology of the different nanowire structures was investigated by SEM at a 30° tilting angle. Figure 1 shows SEM images of the InAs core-only (figure 1a) and the InAs-GaSb core-shell structure (figure 1b) along with schematics of both cases as insets.
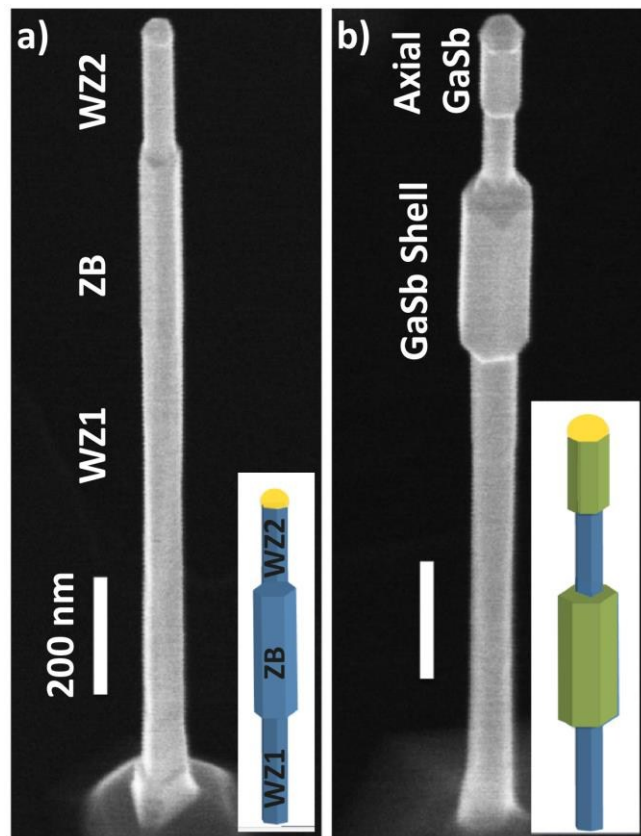
Figure 1: 30°-tilted SEM images of a a) core InAs structure and b) a core-shell structure with the GaSb shell only formed on the zinc blende segment. The insets are schematic demonstrations of the related nanowires, with InAs shown in blue and GaSb in green. As discussed in detail in section (I), under certain conditions an axial GaSb segment is also formed in addition to the shell.

From figure 1a a diameter increase from the WZ to the ZB segment of the InAs core can be seen. This as well as the facet rotation from one structure to the other is a result of the

overgrowth on the side facets [38][28]. It is also clear that WZ1 has a larger diameter compared to WZ2. This occurs when the excess InAs material nucleates and overgrows on WZ1 side facets during the rest of the core growth time. This overgrowth will - as expected from the previous studies - continue the same crystal structure of the underlying nanowire, wurtzite in this case. These diameter differences and facet rotations are also schematically depicted in the insets in figure 1. Note also that the nucleation segment at the base (which has frequent stacking defects) has the same facets as WZ1, so these cannot be distinguished. The overgrowth observed on the WZ1 and nucleation (stem) section results in more and rougher side facets, which will in turn affect radial overgrowth. For this reason, WZ2 is used for comparison with the ZB segment in order to understand the overgrowth of GaSb. As seen in figure 1b, the InAs-GaSb core-shell ZB segment is drastically larger in diameter compared to WZ segment and the pure InAs core structure. From this we can tentatively conclude that the GaSb shell has preferentially formed on the ZB segment. Moreover, it is observed that an axial GaSb segment grows on the top of the second WZ segment mainly for wires with a larger diameter (40 nm) for most of the growth conditions that have been studied, and in some cases for smaller diameters (30 nm) [39]. For more information on the GaSb material composition of this segment please see image S5 of the supplementary information file. The thickness and length of this segment varies with the growth conditions, as will be discussed in later sections.

Thereafter, the samples grown under reference parameters were characterized by high resolution TEM and XEDS analysis, which confirm the presence of a GaSb shell radially grown on the zinc blende segment. The thickness of this shell was measured to be about 8nm, which we will demonstrate as completely controllable by the set parameters of the growth conditions. Figure 2 demonstrates high-resolution TEM with STEM-XEDS analysis for nanowires with Au aerosol particle diameters of 40 nm (figure 2a, b, c, and d) and 30 nm (figure 2e and f) with an areal density of 1 μm^{-2}. The XEDS map in figure 2c implies that a GaSb shell exists around the zinc blende segment. In figure 2b the transition from WZ1 to ZB is emphasized with the white dashed line. The sharp transition from one structure to the next, along with an almost equally sharp transition in shell formation, highlights the control, and potential, of the template method. In the high resolution TEM image shown in figure 2d, regularly twinned segments of the core-shell zinc blende segment can be observed. The position of the edge between the InAs core and GaSb shell, indicated by red dots, can be seen as a change in contrast accompanied by a faint line indicating slight interfacial strain. That this contrast change is correlated with the change of material can be verified by EDX.

Figures e and f show an overview and a high resolution TEM image, respectively, of the zinc blende segment of a nanowire from a different sample, where the intended pure ZB segment contains instead a mixture of ZB and WZ with frequent stacking defects, due to incomplete optimization of the core growth procedure. In figure 2f the approximate transition from InAs to GaSb is indicated by a red dashed line; note however that due to changing facets the interface is not constant in projection and the indication is therefore approximate. Take note how the structural mixing has affected the GaSb shell growth (red and green dashed lines in figure 2f); unevenness is evident in the shell upon this faulty segment. Here, the surface

of the shell is much rougher, with shell thickness varying correlated to the underlying structure. The roughness observed in figure 2f can be explained by the higher radial growth rate of the zinc blende crystal phase for both InAs and GaSb, but is also exacerbated by the 30 ° facet rotations between consecutive ZB and WZ segments which is due to the terminating side facets of wurtzite ({10-10}-type), and zinc blende ({110}-type) structures. This facet rotation results in inclined micro-facets at the interfaces between phases (see [28] for details), which typically have higher surface energies than the flat ZB and WZ facets, yielding uneven surface growth when segments are short. A quick comparison of figures 2d and f signifies the importance of the control over the growing crystal phase along the core nanowire. This precise control is well demonstrated in figure 2g where a very short WZ segment is designed and grown in between two optimized ZB structures. From the HRTEM image it is clear there are no stacking defects at either transitions between the two structures.

To attain a deeper understanding of the processes controlling the selectivity of the GaSb radial growth, as well as to optimize this selectivity, different series were grown in order to map out the growth conditions of the radial GaSb shell on the zinc blende segment. From these we observe significant effects of the temperature and GaSb V/III ratio, which are described in

the following subsections. The total precursor flow did not significantly affect the growth; more information can be found in the supplementary file (S2). The time dependence of the shell growth is also shown in supplementary S3. All these series were compared to the conditions of the reference shell growth described earlier. For the statistical analysis the software NanoDim [40] was used to determine the dimensions of more than 30 nanowires for each sample. The plots have been normalized to the diameter of the upper wurtzite segment (WZ2) for each sample to compensate for the Au aerosol nanoparticle diameter spread when comparing the samples. The WZ1 and ZB diameters of pure InAs core nanowires are also added as a reference for comparison.

II. Temperature dependence of GaSb shell growth

After growing the InAs core at 460 °C, the set temperature was investigated in a range between 420 °C- 500 °C in steps of 20 °C. Several qualitative trends can be observed from the SEM images shown in figure 3a-e.
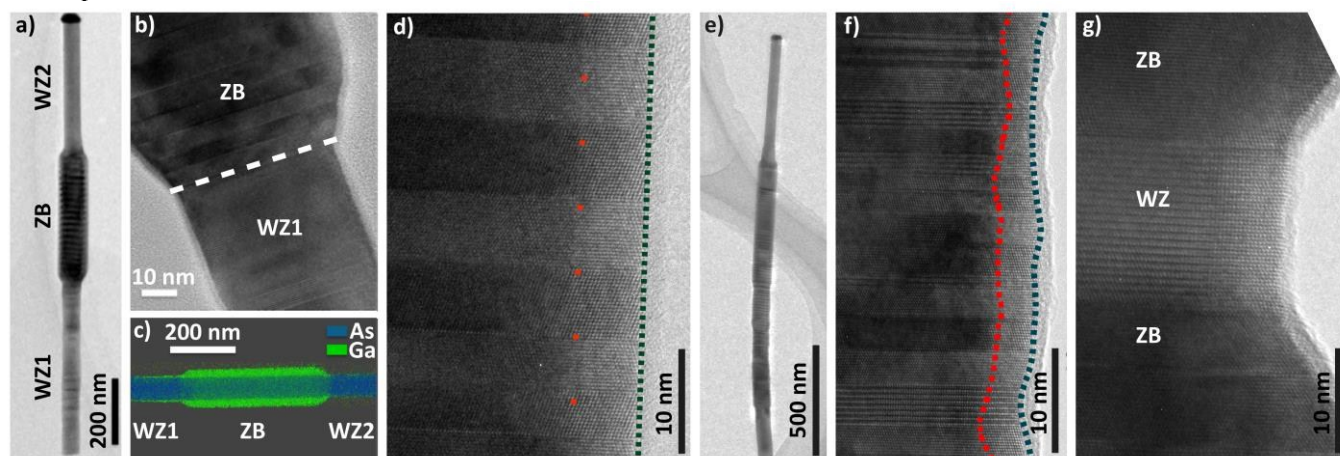
Figure 2: a) TEM bright field (BF) image of a core-shell nanowire grown from a 40 nm Au particle at 460 °C, with a shell V/III ratio of 0.5, with a growth time equal to 20 minutes. b) TEM BF image demonstrating the transition from the WZ1 segment of a nanowire to ZB. c) STEM-XEDS color map of the zinc blende segment of the same wire. It is clear that the GaSb shell has grown preferentially on the zinc blende segment. d) HRTEM image from the same wire where a smooth shell is observable on the regularly twinned zinc blende structure. The green dashed line shows the interface between the shell and the native oxide layer/carbon deposits on the nanowire, whereas the red dashed line shows the approximate position of the interface between the InAs core and the GaSb shell as determined from the contrast change in the HRTEM image. It should be noted that the exact position of the interface cannot be determined in a <110> direction, as the nanowires have (110) side facets and thus the transition represents an edge rather than a facet. (e) An overview TEM image of a nanowire grown from a 30 nm Au seed particles with a faulty zinc blende segment. f) HRTEM image from a section of the same mixed structured InAs core/GaSb shell nanowire as in e), demonstrating the uneven shell caused by the underlying mixed core structure. The green dashed line indicates the border between the GaSb shell and the native oxide layer/carbon deposit, and the red dashed line represents the approximate position of the InAs/GaSb interface. g) HRTEM image of a WZ inset in between two ZB structures demonstrating the high precision and control in growing crystal phase engineered nanowires. From the image it is clearly observable that the transitions between the structures on either side are clean and defect free.

The nanowires consist of 4 distinct segments, corresponding to the three InAs segments and the axial GaSb segment, as shown in Figure 1b. The axial GaSb segment clearly increases in length with increasing growth temperature, but the diameters of the various segments are nearly constant. This happens while

the relative length of WZ2 decreases. This could be related to the higher decomposition rate of the InAs nanowires at higher temperatures by the seed particle in the absence of ambient AsH₃ pressure [20]. At 500 °C, we speculate that the InAs segment has been completely decomposed, and as the two GaSb growth fronts merge the initial segmented morphology of

the nanowires is lost. We also speculate that for a high number of the nanowires the sudden dominance of the GaSb growth causes a change in the wetting angel of the particle, causing the nanowires to kink in a different direction than the conventional <111>B-type growth direction [41].

The diameter of each segment is plotted in figure 3f for temperatures up to 480 °C, together with the reference diameters for the core WZ1 and ZB segments, and the axial GaSb length is shown in figure 3g. The diameter of the ZB segment is nearly constant, indicating that the GaSb radial growth is nearly independent of temperature. This observation is also supported by the constant diameter of the axial GaSb segment of the wire for the studied temperature range. The WZ1 diameter is larger at lower GaSb growth temperatures, with a gradual decrease for increasing temperature, implying thin shell formations on wurtzite side facets at lower temperature ranges. Here we note, as shown in figure 1b, that the WZ1 diameter is similar to or slightly smaller than the ZB diameter, so the increased thickness after shell growth at low temperatures is significant. The slight temperature dependence in thickness for the ZB and WZ1 segments is similar, indicating that the selectivity of the shell growth between the segments cannot be efficiently tuned with temperature. It should also be noted that the stem segment used for nucleation has frequent stacking defects which have in numerous other studies been shown to act as preferential nucleation sites, enhancing radial growth (see for example [39]). Since the stem and WZ1 share common side facets, this will also enhance the radial over growth on the WZ1 up to where the ZB starts. This was the case even for radial growth of InAs (figure 1b), but for lower temperatures also affects overgrowth of GaSb.

III. Dependence of shell growth on V/III ratio of TMGa and TMSb precursors

The V/III ratio of the shell precursors was changed between 0.25 and 3.5 under the same total precursor flow as the reference run; see figure 4a-e. This was done by changing both the TMGa and TMSb molar fractions simultaneously to guarantee constant total precursor flow, as it is a growth variable that has a big impact on nanowire growth and crystal structure. As seen in figure 4f, as the V/III ratio increases from 0.5, the radial growth of GaSb on the ZB segment drastically decreases (indicated by a decreasing total diameter), while the diameter of the axial GaSb segment increases. The length of the axial GaSb segment increases as the V/III ratio of the shell increases to 1.6, where after it drops to lower values again (figure 4g). This observation is well in line with previous studies on axial GaSb growth under different V/III ratios in the same reactor reporting on the narrow axial growth window of GaSb with V/III ratios around 1 [42]. It is also consistent with previous observations of GaSb axial growth on InAs, where nucleation of the GaSb segment was very sensitive to Sb partial pressure [39]. The opposing trends for the shell growth on the InAs ZB segment, and the GaSb axial and radial growth rates suggest a competition for material between the shell and the GaSb segment. The result is that at low V/III, when axial GaSb growth is suppressed, shell growth on zinc blende InAs is maximized. At the same time, the WZ1 diameter curve is constant for the different V/III ratios at a diameter very similar to the expected core diameter (the slight increase in the mid points are explained by the larger standard deviation depicted using the error bars). Low V/III ratio thus gives very good selectivity for growth of a GaSb shell on the ZB segment.
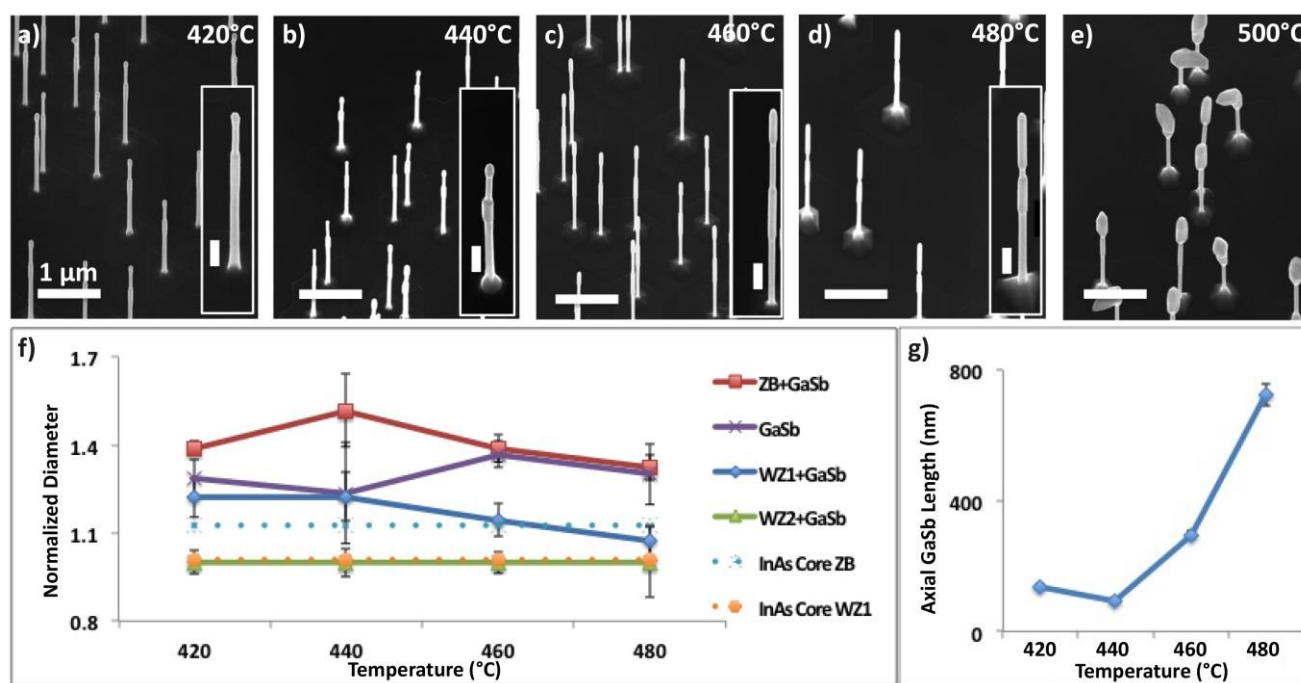
Figure 3: Temperature series of the GaSb shell grown at a) 420 °C, b) 440 °C, c) 460 °C, d) 480 °C, and e) 500 °C. The V/III ratio is kept constant at 1.6. The scale bar corresponds to 1 μm. f) Diameter of different segments versus shell growth temperature. Note that the diameters have been normalized to the diameter of WZ2. g) Length of the axial GaSb segment at different temperatures. It is clear that the growth rate increases at higher temperatures.

Journal Name

RSCPublishing

It is worth noting that for V/III ratios below 0.5 the yield of straight nanowires decreases drastically (figure 4a). We speculate that the kinking occurs in the presence of excessive group III (Ga) atoms in

the seed particle during the shell growth, and the decomposition of the InAs core.
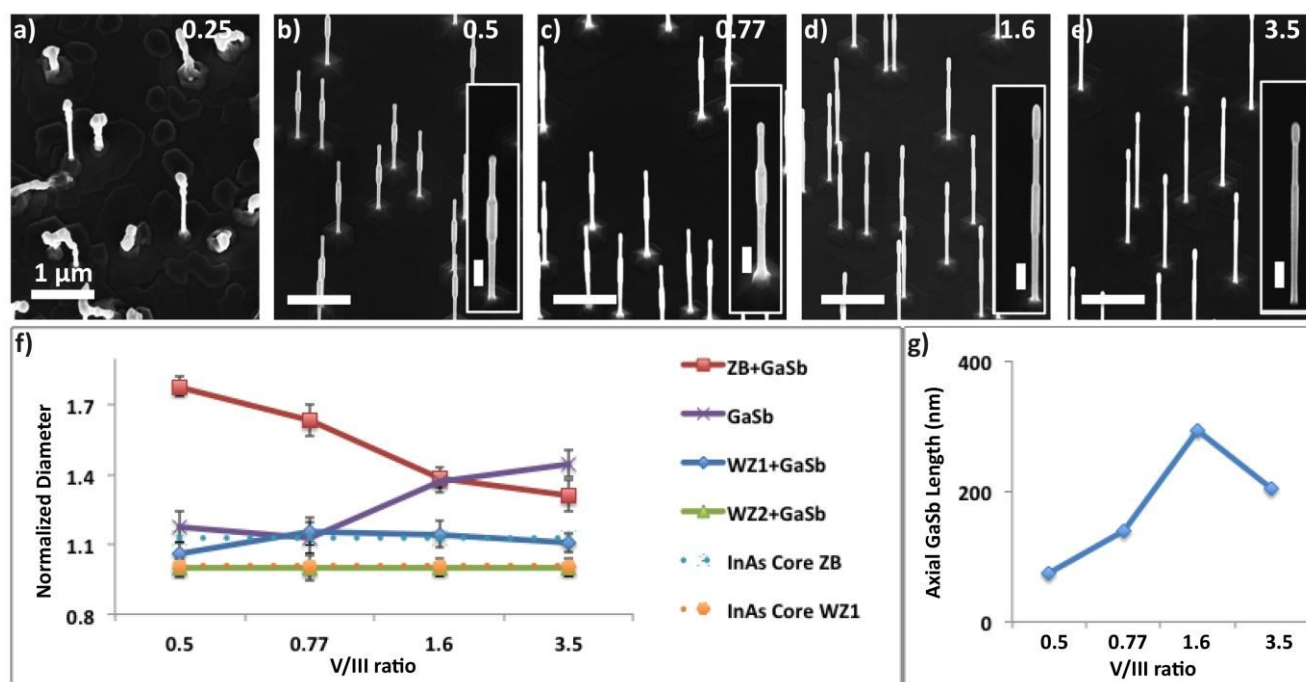
Figure 4: V/III ratio series tested for the GaSb shell. The V/III ratio is varied between a) 0.25, b) 0.5, c) 0.77, d) 1.6, and e) 3.5 while the growth temperature is kept constant at 460°C. The scale bar corresponds to 1μm. f) Normalized diameter of different nanowire segments versus shell V/III ratio. g) Length of the axial GaSb segment at different V/III ratios.

IV.   Multi-structured core-shell nanowires

To further demonstrate the potential and level of control that can be achieved for the GaSb shell growth on well-defined InAs zinc blende crystal structures, we show nanowires in figure 5 which were grown from 30 nm Au particles with three zinc blende segments separated by two very thin wurtzite segments (in addition to the base- and top segments of the nanowires). As seen in the overview SEM image in figure 5a we have achieved a very high yield of straight nanowires and well-defined core-shell segments with varying lengths. The length and positioning of these segments are precisely controlled by tailoring the crystal structure and growth time of the InAs core nanowire segments – a false colored inset is given in figure 5a, highlighting the different segments. Two wurtzite segments with lengths on the order of 15-20 nm are separated by three zinc blende segments of approximate 300 nm in length as GaSb shown in the TEM bright field image viewed along a $<11\overline{2}>$-type direction (figure 5b), and the dark field images acquired along a $<21\overline{3}>$- type direction using wurtzite and zinc blende characteristic diffraction spots (figure

5c). These are merged conventional dark field images of wurtzite (red) and the two 180° rotational zinc blende twins (green) which are given for the identical segment as shown in figure 5b. Higher magnification images of the two wurtzite segments viewed along the $<11\overline{2}>$–type direction are given in figure 5d, with color coding for the wurtzite and zinc blende segments as revealed by overlaying the images taken along $<11\overline{2}>$-type and $<21\overline{3}>$- type directions. Here it is worth noting that the zinc blende and wurtzite characteristic bilayer stacking cannot be distinguished for $<11\overline{2}>$-type viewing directions but is possible for the $<21\overline{3}>$- type directions perpendicular to the $<\overline{111}>$–type growth direction). The subsequently smaller nanowire diameter at the position of the wurtzite segments is attributed to the selective GaSb shell growth, which almost exclusively forms on the zinc blende facets/segments, as demonstrated by the XEDS analysis in figures 5e-g. These images are taken along the $<11\overline{2}>$–type direction for identical nanowire as shown in figures 5b-d. This precise control can be used in various device configurations, such as interband tunnel diodes and transistors, in order to have

Nanoscale Accepted Manuscript

carrier injection from the shell into the core exclusively at a desired position and length of the nanowire.
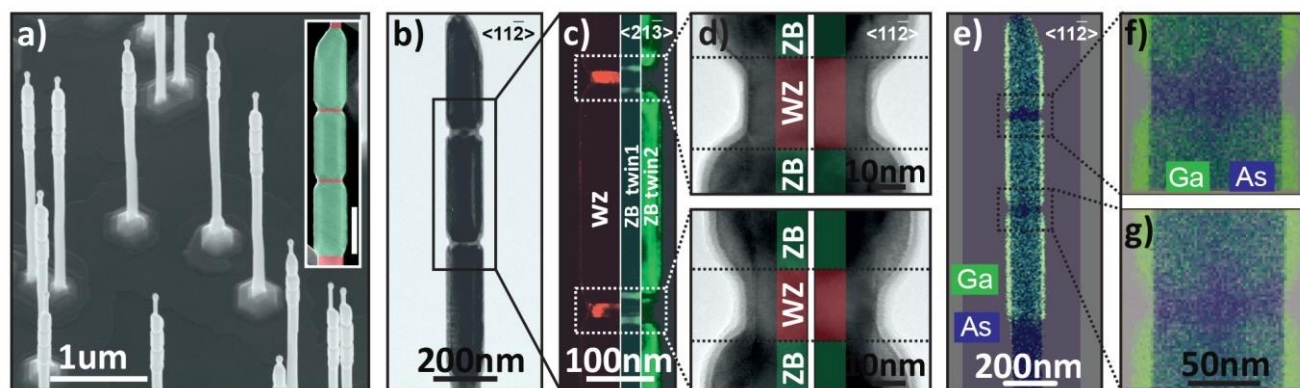
Figure 5: a) SEM image of InAs-GaSb core-shell nanowires grown from nominally 30 nm aerosol particles with multiple, axially stacked zinc blende and wurtzite segments. The inset displays a false colored (wurtzite – red, zinc blende – green) higher magnification side view of one representative nanowire (scale bar 200 nm). b) TEM bright field image of a nanowire section similar to the inset given in a) demonstrated the two WZ segments with smaller diameters. c) Merged conventional dark field images of the wurtzite, and the two zinc blende twins given in red and green respectively. d) Higher magnification images of the two WZ segments color coded by overlaying the images taken along $<11\bar{2}>$-type and $<21\bar{3}>$- type directions. e) An XEDS map of characteristic Ga (indicative of the GaSb shell) and As (indicative of the InAs core) taken for an identical nanowire as shown in (b-d), with higher magnification views of the two wurtzite segments embedded in zinc blende in f) and g) highlighting the selectivity of the GaSb shell growth.

V.   Electrical measurements

SEM images, before and after contact processing, of an InAs-GaSb core-shell nanowire used in the electrical measurements are displayed in figure 6a. The electrical properties of the ZB and WZ1 segments were investigated by measuring the drain current as a function of gate voltage. The bare InAs reference sample was measured at room temperature and with a drain bias of 10 mV, whereas the sample with selective GaSb overgrowth were measured at both room temperature and 4.2 K with a drain bias of 1 mV, see figure 6b-d. Starting with the reference sample (figure 6b), we note that the conductance of the ZB and WZ1 segments show similar gate voltage dependence. Going to negative gate voltages deplete the nanowire segments from charge carriers, which is expected since nominally intrinsic InAs material with a large surface-to-volume ratio, shows n-type behavior [43]. The current level is higher for ZB, which we attribute to a larger physical diameter and a higher charge carrier density compared with WZ. Looking next at the core-

shell sample in figure 6a, we note that the measurements on the ZB segment (figure 6c) do not show the characteristics of bare InAs. Instead, the segment shows ambipolar transport characteristics, which can be attributed to an onset of hole transport in the GaSb shell at negative gate voltages, see inset in figure 2c. A similar ambipolarity has been observed and extensively studied in the reverse core-shell system (GaSb-InAs) [42]. By contrast, the WZ1 segment depletes at negative gate voltages, and has a conductance trace very similar to the reference segment, consistent with suppression of shell growth on wurtzite surface facets. As can be seen in figure 6d, the ambipolar characteristics is even more pronounced at T = 4.2 K. The light blue dashed line indicates extrapolated conductance of a corresponding ZB segment without a shell of GaSb.
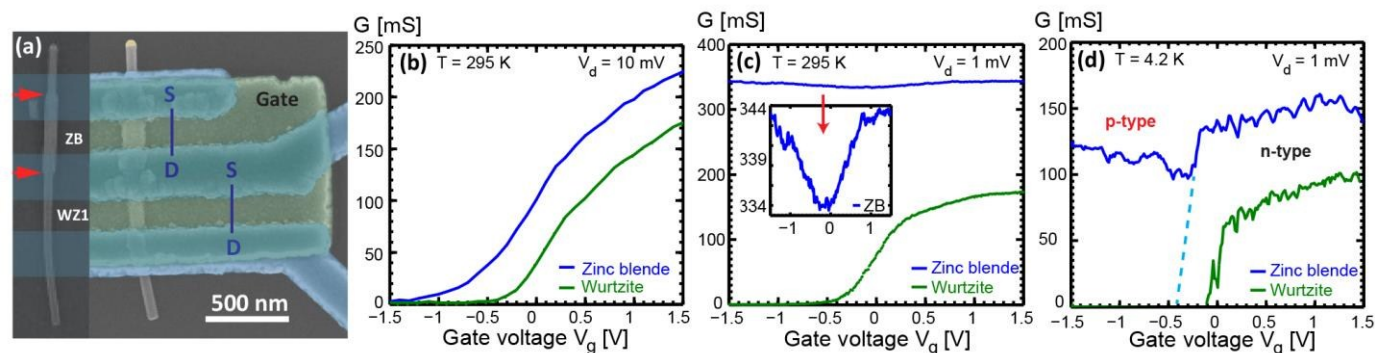
Figure 6: a) (left) SEM image of the nanowire prior to device fabrication, the red arrows indicate the transitions between WZ1 and ZB segments and the blue shadowed areas indices where the source- and drain contacts will be located. (right) False-colored SEM image of the completed device where source-/drain- and gate contacts are colored blue and green, respectively. Conductance as a function of gate voltage of ZB (blue) and WZ (green) segments in nanowires. b) Reference InAs wire, not exposed to GaSb growth, measured at room temperature. c) InAs wire with GaSb shell on the zinc blende segment shown in panel (a) measured at room temperature. The inset is a magnification of the data for the zinc blende segment. d) Same nanowire as in panel (c) measured at $T = 4.2$ K.

Summary

In this study we have demonstrated and investigated the selective radial growth of GaSb on chosen surfaces along the length of an InAs core nanowire. This was realized by controlled crystal phase engineering and utilizing the higher surface energy of zinc blende structures compared to wurtzite, leading to a higher radial growth rate under optimized conditions. We have mapped out the dependence of the selective shell growth on the growth temperature, V/III ratio, total precursor flow, and growth time. From these investigations we conclude that: (i) The radial GaSb growth on the zinc blende segment is nearly independent of growth temperature, while the undesired GaSb overgrowth on the wurtzite segment decreases with increasing temperature. (ii) Within a V/III ratio window of 0.5 to 3.5, the GaSb radial overgrowth on the zinc blende segment drastically drops with increasing V/III ratio, while no considerable GaSb overgrowth is observable on the wurtzite segment. Using the obtained knowledge we further demonstrate the fabrication of multiple position-controlled core-shell segments along the length of the nanowires under optimized shell growth conditions. This unique overgrowth method could be applied to any heteroepitaxial material system which exhibits different surface energies for the wurtzite and zinc blende crystal structures.

Electrical measurements show ambipolar (*p*- and *n*-) transport characteristics of the zinc blende segments in core-shell nanowires, whereas the wurtzite segments only show *n*-type transport, similar to bare reference InAs nanowires. These findings are consistent with selective radial growth of *p*-type GaSb on zinc blende InAs surface facets. Taking these findings into account, we anticipate that the template method demonstrated in this work is of considerable interest for quantum transport studies, as it allows for precise epitaxial control of core-shell quantum-dot-like structures.

Acknowledgements

Notes and references

[a] Solid State Physics, Lund University, Box 118, S-221 00 Lund, Sweden.
[b] Center for Analysis and Synthesis, Lund University, Box 124, S-221 00 Lund, Sweden.

Electronic Supplementary Information (ESI) available: S1. Optimization of InAs core crystal structure, S2. Time dependence of GaSb shell growth S3. Total precursor flow influence on GaSb shell growth
See DOI: 10.1039/b000000x/

[1] E. D. Minot, F. Kelkensberg, M. van Kouwen, J. A. van Dam, L. P. Kouwenhoven, V. Zwiller, M. T. Borgström, O. Wunnicke, M. A. Verheijen, and E. P. A. M. Bakkers, "Single quantum dot nanowire LEDs.," *Nano Lett.*, vol. 7, no. 2, pp. 367–71, Feb. 2007.

[2] A. W. Dey, J. Svensson, M. Ek, E. Lind, C. Thelander, and L.-E. Wernersson, "Combining axial and radial nanowire heterostructures: radial Esaki diodes and tunnel field-effect transistors.," *Nano Lett.*, vol. 13, no. 12, pp. 5919–24, Jan. 2013.

[3] J. C. Johnson, H.-J. Choi, K. P. Knutsen, R. D. Schaller, P. Yang, and R. J. Saykally, "Single gallium nitride nanowire lasers.," *Nat. Mater.*, vol. 1, no. 2, pp. 106–10, Oct. 2002.

[4] P. Krogstrup, H. I. Jørgensen, M. Heiss, O. Demichel, J. V. Holm, M. Aagesen, J. Nygard, and A. Fontcuberta i Morral, "Single-nanowire solar cells beyond the Shockley–Queisser limit," *Nat. Photonics*, vol. 7, no. 4, pp. 306–310, Mar. 2013.

[5] S. Nadj-Perge, S. M. Frolov, E. P. A. M. Bakkers, and L. P. Kouwenhoven, "Spin-orbit qubit in a semiconductor nanowire.," *Nature*, vol. 468, no. 7327, pp. 1084–7, Dec. 2010.

[6] B. Piccione, C.-H. Cho, L. K. van Vugt, and R. Agarwal, "All-optical active switching in individual semiconductor nanowires.," *Nat. Nanotechnol.*, vol. 7, no. 10, pp. 640–5, Oct. 2012.

[7] K. Tomioka, M. Yoshimura, and T. Fukui, "A III-V nanowire channel on silicon for high-performance vertical transistors.," *Nature*, vol. 488, no. 7410, pp. 189–92, Aug. 2012.

[8] R. Yan, D. Gargas, and P. Yang, "Nanowire photonics," *Nat. Photonics*, vol. 3, no. 10, pp. 569–576, Oct. 2009.

[9] J. Johansson and K. A. Dick, "Recent advances in semiconductor nanowire heterostructures," *CrystEngComm*, vol. 13, no. 24, p. 7175, Nov. 2011.

[10] P. Krogstrup, J. Yamasaki, C. B. Sørensen, E. Johnson, J. B. Wagner, R. Pennington, M. Aagesen, N. Tanaka, and J. Nygård, "Junctions in axial III-V heterostructure nanowires obtained via an interchange of group III elements.," *Nano Lett.*, vol. 9, no. 11, pp. 3689–93, Nov. 2009.

[11] N. Li, T. Y. Tan, and U. Gösele, "Transition region width of nanowire hetero- and pn-junctions grown using vapor–liquid–solid processes," *Appl. Phys. A*, vol. 90, no. 4, pp. 591–596, Jan. 2008.

[12] C.-Y. Wen, M. C. Reuter, J. Bruley, J. Tersoff, S. Kodambaka, E. A. Stach, and F. M. Ross, "Formation of compositionally abrupt axial heterojunctions in silicon-germanium nanowires," *Science*, vol. 326, no. 5957, pp. 1247–50, Nov. 2009.

Nanoscale Accepted Manuscript

[13] R. E. Algra, M. Hocevar, M. A. Verheijen, I. Zardo, G. G. W. Immink, W. J. P. van Enckevort, G. Abstreiter, L. P. Kouwenhoven, E. Vlieg, and E. P. A. M. Bakkers, "Crystal structure transfer in core/shell nanowires.," *Nano Lett.*, vol. 11, no. 4, pp. 1690–4, Apr. 2011.

[14] L. J. Lauhon, M. S. Gudiksen, D. Wang, and C. M. Lieber, "Epitaxial core-shell and core-multishell nanowire heterostructures.," *Nature*, vol. 420, no. 6911, pp. 57–61, Nov. 2002.

[15] S. K. Lim, M. J. Tambe, M. M. Brewster, and S. Gradecak, "Controlled growth of ternary alloy nanowires using metalorganic chemical vapor deposition.," *Nano Lett.*, vol. 8, no. 5, pp. 1386–92, May 2008.

[16] T. J. Kempa, S.-K. Kim, R. W. Day, H.-G. Park, D. G. Nocera, and C. M. Lieber, "Facet-selective growth on nanowires yields multi-component nanostructures and photonic devices.," *J. Am. Chem. Soc.*, vol. 135, no. 49, pp. 18354–7, Dec. 2013.

[17] T. Rieger, T. Schäpers, D. Grützmacher, and M. I. Lepsa, "Crystal Phase Selective Growth in GaAs/InAs Core–Shell Nanowires," *Cryst. Growth Des.*, vol. 14, no. 3, pp. 1167–1174, Mar. 2014.

[18] J. Wallentin, M. E. Messing, E. Trygg, L. Samuelson, K. Deppert, and M. T. Borgström, "Growth of doped InAsyP1−y nanowires with InP shells," *J. Cryst. Growth*, vol. 331, no. 1, pp. 8–14, Sep. 2011.

[19] S. G. Ghalamestani, A. M. Munshi, D. L. Dheeraj, B.-O. Fimland, H. Weman, and K. A. Dick, "Self-catalyzed MBE grown GaAs/GaAs(x)Sb(1-x) core-shell nanowires in ZB and WZ crystal structures.," *Nanotechnology*, vol. 24, no. 40, p. 405601, Oct. 2013.

[20] S. Gorji Ghalamestani, M. Heurlin, L.-E. Wernersson, S. Lehmann, and K. A. Dick, "Growth of InAs/InP core-shell nanowires with various pure crystal structures.," *Nanotechnology*, vol. 23, no. 28, p. 285601, Jul. 2012.

[21] K. a. Dick, J. Bolinsson, M. E. Messing, S. Lehmann, J. Johansson, and P. Caroff, "Parameter space mapping of InAs nanowire crystal structure," *J. Vac. Sci. Technol. B Microelectron. Nanom. Struct.*, vol. 29, no. 4, p. 04D103, 2011.

[22] P. Caroff, K. A. Dick, J. Johansson, M. E. Messing, K. Deppert, and L. Samuelson, "Controlled polytypic and twin-plane superlattices in iii-v nanowires.," *Nat. Nanotechnol.*, vol. 4, no. 1, pp. 50–5, Jan. 2009.

[23] J. Bolinsson, P. Caroff, B. Mandl, and K. A. Dick, "Wurtzite-zincblende superlattices in InAs nanowires using a supply interruption method.," *Nanotechnology*, vol. 22, no. 26, p. 265606, Jul. 2011.

[24] R. E. Algra, M. A. Verheijen, M. T. Borgström, L.-F. Feiner, G. Immink, W. J. P. van Enckevort, E. Vlieg, and E. P. A. M. Bakkers, "Twinning superlattices in indium phosphide nanowires.," *Nature*, vol. 456, no. 7220, pp. 369–72, Nov. 2008.

[25] P. Caroff, J. Bolinsson, and J. Johansson, "Crystal Phases in III--V Nanowires: From Random Toward Engineered Polytypism," *IEEE J. Sel. Top. Quantum Electron.*, vol. 17, no. 4, pp. 829–846, Jul. 2011.

[26] H. J. Joyce, J. Wong-Leung, Q. Gao, H. H. Tan, and C. Jagadish, "Phase perfection in zinc Blende and Wurtzite III-V nanowires using basic growth parameters.," *Nano Lett.*, vol. 10, no. 3, pp. 908–15, Mar. 2010.

[27] H. Huang, X. Ren, X. Ye, J. Guo, Q. Wang, X. Zhang, S. Cai, and Y. Huang, "Control of the crystal structure of InAs nanowires by tuning contributions of adatom diffusion.," *Nanotechnology*, vol. 21, no. 47, p. 475602, Nov. 2010.

[28] S. Lehmann, J. Wallentin, D. Jacobsson, K. Deppert, and K. A. Dick, "A general approach for sharp crystal phase switching in InAs, GaAs, InP, and GaP nanowires using only group V flow.," *Nano Lett.*, vol. 13, no. 9, pp. 4099–105, Sep. 2013.

[29] B. Ganjipour, M. Ek, B. Mattias Borg, K. A. Dick, M.-E. Pistol, L.-E. Wernersson, and C. Thelander, "Carrier control and transport modulation in GaSb/InAsSb core/shell nanowires," *Appl. Phys. Lett.*, vol. 101, no. 10, p. 103501, Sep. 2012.

[30] T. Rieger, D. Grützmacher, and M. I. Lepsa, "Misfit dislocation free InAs/GaSb core-shell nanowires grown by molecular beam epitaxy," *Nanoscale*, Nov. 2014.

[31] A. W. Dey, B. M. Borg, B. Ganjipour, M. Ek, K. A. Dick, E. Lind, C. Thelander, and L.-E. Wernersson, "High-Current GaSb/InAs(Sb) Nanowire Tunnel Field-Effect Transistors," *IEEE Electron Device Lett.*, vol. 34, no. 2, pp. 211–213, Feb. 2013.

[32] B. M. Borg, K. A. Dick, B. Ganjipour, M.-E. Pistol, L.-E. Wernersson, and C. Thelander, "InAs/GaSb heterostructure nanowires for tunnel field-effect transistors.," *Nano Lett.*, vol. 10, no. 10, pp. 4080–5, Oct. 2010.

[33] I. Knez, R.-R. Du, and G. Sullivan, "Evidence for Helical Edge Modes in Inverted InAs/GaSb Quantum Wells," *Phys. Rev. Lett.*, vol. 107, no. 13, p. 136603, Sep. 2011.

[34] C. Liu, T. Hughes, X.-L. Qi, K. Wang, and S.-C. Zhang, "Quantum Spin Hall Effect in Inverted Type-II Semiconductors," *Phys. Rev. Lett.*, vol. 100, no. 23, p. 236601, Jun. 2008.

[35] B. Ganjipour, M. Leijnse, L. Samuelson, H. Q. Xu, and C. Thelander, "Transport studies of electron-hole and spin-orbit interaction in GaSb/InAsSb core-shell nanowire quantum dots," *Phys. Rev. B*, vol. 91, no. 16, p. 161301, Apr. 2015.

[36] V. Pankoke, P. Kratzer, and S. Sakong, "Calculation of the diameter-dependent polytypism in GaAs nanowires from an atomic motif expansion of the formation energy," *Phys. Rev. B*, vol. 84, no. 7, p. 075455, Aug. 2011.

[37] N.V. Sibirev, M.A. Timofeeva, A.D. Bol'shakov, M.V. Nazarenko, V.G. Dubrovskii, "Surface energy and crystal structure of nanowhiskers of III-V semiconductor compounds", *Phys. Solid State*, vol. 52, no. 5, p. 1531, 2010

[38] T. Xu, K. A. Dick, S. Plissard, T. H. Nguyen, Y. Makoudi, M. Berthe, J.-P. Nys, X. Wallart, B. Grandidier, and P. Caroff, "Faceting, composition and crystal phase evolution in III-V antimonide nanowire heterostructures revealed by combining microscopy techniques.," *Nanotechnology*, vol. 23, no. 9, p. 095702, Mar. 2012.

[39] M. Ek, B. M. Borg, J. Johansson, and K. A. Dick, "Diameter limitation in growth of III-Sb-containing nanowire

heterostructures.," *ACS Nano*, vol. 7, no. 4, pp. 3668–75, Apr. 2013.

[40]   NanoDim Software, *http://www.nanodim.net*

[41]   B. Mattias Borg and L.-E. Wernersson, "Synthesis and properties of antimonide nanowires.," *Nanotechnology*, vol. 24, no. 20, p. 202001, May 2013.

[42]   M. Jeppsson, K. a. Dick, J. B. Wagner, P. Caroff, K. Deppert, L. Samuelson, and L.-E. Wernersson, "GaAs/GaSb nanowire heterostructures grown by MOVPE," *J. Cryst. Growth*, vol. 310, no. 18, pp. 4115–4121, Aug. 2008.

[43]   C. Thelander, M. T. Björk, M. W. Larsson, A. E. Hansen, L. R. Wallenberg, and L. Samuelson, "Electron transport in InAs nanowires and heterostructure nanowire devices," *Solid State Commun.*, vol. 131, no. 9–10, pp. 573–579, Sep. 2004.